Production cross sections of proton-rich ^{70}Ge fragments and the decay of ^{57}Zn and ^{61}Ge

B. Blank[1], C. Borcea[2] G. Canchel[1], C.-E. Demonchy[1], F. de Oliveira Santos[3], C. Dossat[4], J. Giovinazzo[1], S. Grévy[3], L. Hay[1], P. Hellmuth[1], S. Leblanc[1], I. Matea[1], J.-L. Pedroza[1], L. Perrot[3], J. Pibernat[1], A. Rebii[1], L. Serani[1], and J.C. Thomas[3]

[1] Centre d'Etudes Nucléaires de Bordeaux Gradignan - UMR 5797 CNRS/IN2P3 - Université Bordeaux 1, Chemin du Solarium, BP 120, 33175 Gradignan Cedex, France
[2] Institute of Atomic Physics, P.O. Box MG6, Bucharest-Margurele, Romania
[3] Grand Accélérateur National d'Ions Lourds, B.P. 55027, F-14076 Caen Cedex 05, France
[4] DAPNIA, CEA Saclay, F-91191 Gif-sur-Yvette Cedex, France

the date of receipt and acceptance should be inserted later

Abstract. Proton-rich isotopes of zinc and germanium, ^{57}Zn and ^{61}Ge, have been produced by fragmentation of a ^{70}Ge beam at the LISE3 facility of GANIL. Their main decay characteristics have been studied after implantation in a double-sided silicon strip detector. In addition, the production cross sections of proton-rich isotopes in the copper-to-germanium region have been determined. These cross sections are much lower than predicted by the EPAX formula. These findings question to some extent the production rates expected for present and future fragmentation facilities.

PACS. 21.10.-k Properties of nuclei – 21.10.Tg Lifetimes – 23.50.+z Decay by proton emission – 29.30.Ep Charged-particle spectroscopy

1 Introduction

For many decades, nuclear structure studies were mainly performed with nuclei close to stability. However, since the late 1960s and the 1970s, more and more isotopes far away from stability could be produced either by fragmenting stable-isotope beams at intermediate or relativistic energies or by fusion-evaporation reactions at Coulomb-barrier energies. The fusion-evaporation reactions allowed one to reach the one-proton drip-line, the limit where the nuclear forces are no longer able to bind all protons, up to bismuth. The fragmentation of medium- and high-energy stable-isotope beams on the target of a fragment separator proved to be the most efficient way to produce the even more exotic, i.e. more proton-rich, drip-line nuclei with an even number of protons (see e.g. [1,2]).

However, the production rates with which these latter isotopes can be reached depend strongly on the projectile used. The EPAX parameterization [3] is one of the efforts to predict these production rates reliably. However, as this formula is based on available measured production cross sections and uses extrapolations of trends, the predictive power of the EPAX parameterisation sometimes turns out to be too optimistic. Therefore, measurements are needed in particular in regions where no cross sections were known at the time when this parameterisation was established to validate its predictions.

Once produced, the isotopes far from the valley of stability allow for a detailed test of our understanding of nuclear structure and, if needed, for a modification of our concepts. These tests can be performed either by using these isotopes to induce nuclear reactions or by studying their radioactive decay. The decay studies enable us in particular to test effective interactions in the framework of the shell model.

In the present experiment, we produced proton-rich nuclei in the copper-to-germanium region to measure their production rates, to search for a new candidate for two-proton radioactivity, ^{59}Ge, and to study the decay properties of other nuclei in this region, where β-delayed proton emitters were observed. The super-allowed Fermi β decay populates a state in the β-decay daughter, the isobaric analog state (IAS), which belongs to the isobaric multiplet of the ground state of the β emitter. These two states, together with states in neighboring nuclei of the same mass, form this multiplet and their masses are linked via the isobaric multiplet mass equation (IMME) [4]. To use the IMME for mass extrapolation, three masses of a multiplet must be known in order to predict all the missing masses of the multiplet. If only one or two masses are known, the method of Coulomb displacement energies [5,6] can be used. Another method used below is the Garvey-Kelson approach [7], which allows one to calculate ground-state masses of exotic nuclei by means of known masses of less exotic nuclei. We will use these concepts below to determine the mass of ^{57}Zn and ^{61}Ge.

2 Experimental procedure

The isotopes of interest were produced by projectile fragmentation of a $^{70}Ge^{28+}$ primary beam at 71.6 MeV/nucleon with an average intensity of 2 μA provided by the coupled cyclotrons

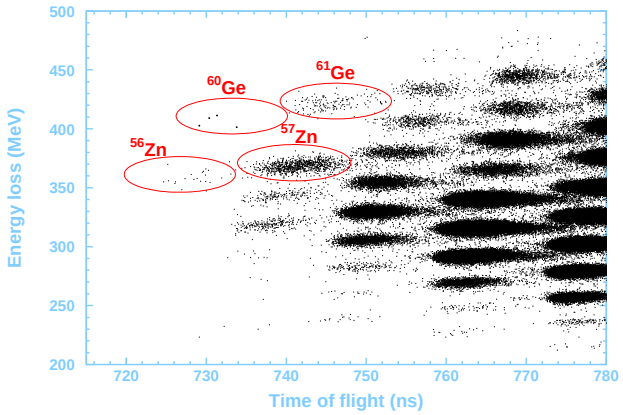

Fig. 1. Two-dimensional identification plot for all the LISE3 settings used in the present experiment. The energy loss in the first silicon detector is plotted as a function of the time of flight between the target and the silicon detectors. Isotopes between arsenic and titanium can be identified. The plot corresponds to the whole experiment of about 3 days of data taking. Details of our identification procedure are given in [9].

of GANIL. This beam was fragmented on a 200μm thick nickel target at the entrance of the LISE3 separator [8]. Nuclei were selected by the LISE3 fragment separator by means of magnetic fields, a beryllium degrader (100μm), and a velocity filter (300 kV). Different settings optimized for ^{59}Ge, for ^{61}Ge, and for ^{63}Ge allowed us to scan the production cross sections for proton-rich isotopes in this region and to study the decay of ^{57}Zn and of ^{61}Ge.

The isotopes which reached the LISE3 focal plane traversed a 100μm thick aluminum degrader foil as well as a set of silicon detectors - a first standard detector (thickness 150μm), a second position-sensitive detector (150μm) with resistive readout, and a third 150μm thick detector - and were finally implanted in a 300μm thick double-sided silicon strip detector (DSSSD) with 16$\times$16 x-y strips and a pitch of 3 mm. Together with two micro-channel-plate detectors (MCPs) at the LISE3 intermediate focal plane, these detectors allowed for an event-by-event identification of ions reaching the LISE3 final focal plane. This identification was performed by means of time-of-flight measurements between the production target (via the radio-frequency of the cyclotrons) and the silicon detectors and between the MCPs and the silicon detectors as well as by means of energy-loss and residual energy measurements with the silicon detectors. Figure 1 shows the identification plot obtained from all the LISE3 settings.

For the decay events, all strips of the DSSSD have been calibrated by means of a triple-α source. The energy shift of the decay events due to pile-up of β-delayed protons and β particles was corrected for by calculating for each isotope the implantation depth with the LISE code [10] and by a Monte-Carlo simulation for the effect of the β particles. We applied a correction of -120 keV for ^{57}Zn and of -100 keV for ^{61}Ge. The effect of the dead layer on the surface of the DSSSD was corrected for by a small correction of the α energies according to the thickness of the dead layer (-50 keV). To account for the uncertainty in determining the latter correction, we add 50 keV quadratically to the uncertainties of the centroids obtained by fitting the peaks of the β-delayed proton spectra. This silicon setup was surrounded by four EXOGAM clovers which yielded a photopeak efficiency of 2.8 % at 1.3 MeV.

Implantation events were triggered by the first silicon detector, whereas decay events were collected, if one of the strips of the DSSSD fired. Due to a rather high trigger threshold for the decay events of about 1.9 MeV, only β-delayed proton events could be observed. Therefore, only the decays of ^{57}Zn and of ^{61}Ge could be studied in the present work. For ^{56}Zn and ^{60}Ge, the statistics in the decay spectra is too low, e.g. in the case of ^{60}Ge only two decay events could be registered. All other nuclei have only very weak β-delayed proton channels and decay mainly by $\beta\gamma$ emission, which did not trigger the data acquisition. Due to their lower thresholds as compared to the other side, only one side of the DSSSD was used through out the present paper, i.e. the DSSSD was in fact used as a single-sided silicon strip detector.

3 Production cross sections

The production cross sections have been determined by means of the number of ions identified, the target thickness, the integrated beam intensity measured with electro-magnetic pick-ups in front of the production target at the entrance of the LISE3 beam line, the transmission of the LISE3 beam line as calculated with the LISE code [10] and a dead-time correction. We determined the cross sections only for ions transmitted close to the central path through the LISE3 separator, for which the transmission estimates are more or less reliable. This means that we took into account only isotopes for which the transmission was above 1%. In addition, we assumed that the transmission has a relative uncertainty of 50%.

Figure 2 shows the cross sections thus obtained. They are compared with EPAX predictions [3]. EPAX is not able to reproduce our experimental data. It overpredicts the production of all isotopes. This result is astonishing as the EPAX formula predicts nicely production cross sections for the fragmentation of other proton-rich stable-isotope beams like ^{92}Mo [11] and ^{58}Ni [12].

The present results are in agreement with results recently obtained at the Coupled Cyclotron Facility of Michigan State University [13]. These authors observed for the first time the proton drip-line nuclei ^{60}Ge and ^{64}Se and determined their production cross sections as well as those of other proton-rich nuclei in this region for fragmentation reactions of a ^{78}Kr beam on a beryllium target. As in the present case, the cross sections predicted by EPAX exceed largely the experimental cross sections. In contrast, predictions by the abrasion-ablation model agreed with the experimental values [13]. In figure 2, when comparing the data of Stolz et al. which were taken with a beryllium target and our results from a nickel target, we observe that for less exotic nuclei the production with a low-Z target yields higher cross sections, whereas for the most proton-rich nuclei the nickel target gives better results.

The cross sections for deep inelastic collisions were found to depend on the Q value for the reaction channel to produce the final fragment, the basic idea being that higher Q values

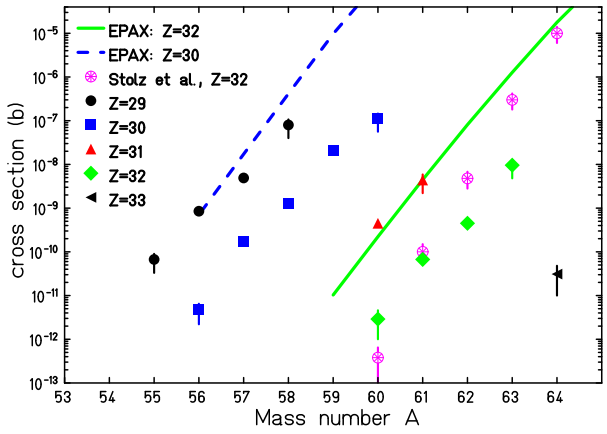

Fig. 2. Production cross sections for projectile fragmentation of a primary ^{70}Ge beam at 71.6 MeV/nucleon on a nickel target. Our experimental data are compared to data from Stolz et al. [13] and to model predictions from EPAX 2 [3]. The full line is the EPAX prediction for ^{70}Ge fragmentation producing germanium (Z=32) isotopes, whereas the dashed line corresponds to the predictions for zinc isotopes (Z=30).

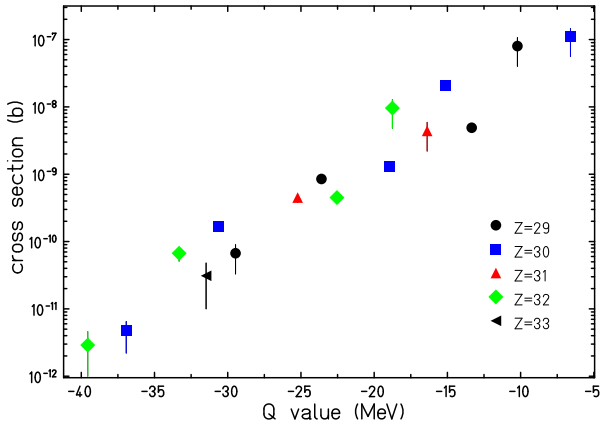

Fig. 3. Plot of the cross sections for projectile fragmentation versus the Q value of the reaction to produce these nuclei in transfer reactions ^{58}Ni(^{70}Ge,^{n}X)^{m}Y. We used Q values from AME03 [15].

are less "economic" for the reaction and therefore less probable (see e.g. [14]). Figure 3 shows a plot of the logarithm of the cross sections as a function of the Q value to reach the different nuclei. As an example, the Q value for the reaction ^{58}Ni(^{70}Ge,^{60}Ge)^{68}Ni is calculated to be -39.6 MeV [15]. Besides an evident odd-even staggering, the data nicely aline along a straight line supporting thus the relation between the logarithm of the cross sections and the Q value.

The present results show that the EPAX formula, although based on a large variety of experimental data, can still be improved. Especially, more and more experimental data for rather low production cross sections exist now and may be included in a new fit or even in a modified parameterisation of EPAX.

Our experimental data for heavier germanium isotopes (see figure 2) allow us also to extrapolate the cross sections to the production cross section of ^{59}Ge, a possible ground-state two-proton emitter. The extrapolated cross section is about 30 fb. This is an extremely low cross section, which might be compared to the production cross section for doubly-magic ^{48}Ni, which was estimated to be about 50 fb [1]. In the case of ^{59}Ge, this production cross section would yield a detection rate of about one nucleus every three days, assuming optimum conditions, i.e. a primary beam intensity of 4μA on the SISSI target and a lifetime sufficiently long to reach the LISE3 focal plane.

4 Experimental results for the decay studies

4.1 The decay of the T_z = -3/2 nucleus ^{57}Zn

The decay-energy and decay-time distributions for ^{57}Zn are shown in figure 4. The decay-energy spectrum shows four well-defined peaks at 1.90(6) MeV, 2.56(5) MeV, 3.13(6) MeV, and 4.59(5) MeV with branching ratios of 14(2)%, 13(2)%, 6(2)%, and 19(2)%. The branching ratio for the low-energy peak is probably biased by the energy cut-off (see below). The high-energy tail of the proton peaks is due to β summing.

Three of these peaks were already observed by Vieira et al. [16] with energies of 1.94(5) MeV, 2.58(5) MeV, and 4.65(5) MeV, and all four by Jokinen et al. [17] with values of 1.90(1) MeV, 2.53(2) MeV, 3.09(2) MeV, and 4.60(3) MeV, in agreement with our energy values. We calculate error-weighted averages of 1.90(1) MeV, 2.54(2) MeV, 3.09(2) MeV, and 4.61(2) MeV.

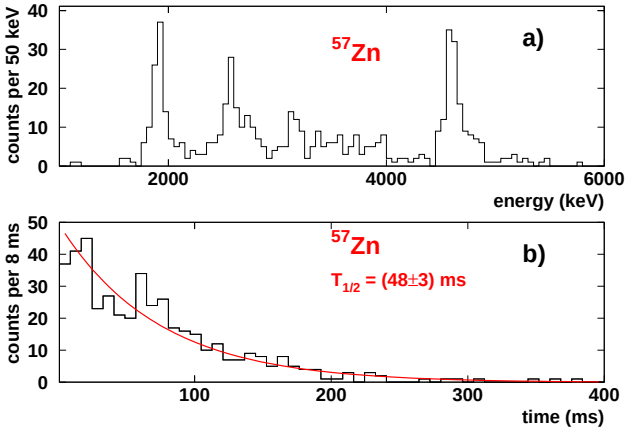

Fig. 4. a) Decay energy spectrum for ^{57}Zn. The proton groups observed belong to the decay of the IAS in ^{57}Cu to the ground state of ^{56}Ni (E_p^{cm} = 4.60 MeV) and to the first excited state (E_p^{cm} = 1.90 MeV) as well as to the decay of Gamow-Teller fed states to the ground state of ^{56}Ni (E_p^{cm} = 2.56 MeV, 3.09 MeV). b) The decay-time spectrum was generated by measuring the time between a ^{57}Zn implantation and subsequent decay events. A fit with an exponential and a constant yields a half-life of 48(3) ms.

We present here for the first time absolute branching-ratio measurements for this nucleus determined from the number

of implanted ^{57}Zn isotopes (1002(50) implantations) and the number of protons observed for the different peaks assuming a 100% proton detection efficiency, expect for the high-energy peak, where a Monte-Carlo simulation taking into account the implantation depth in the DSSSD yields 85%. Only rough estimates for the branching ratios were given in the work of reference [16], based on an assumed log ft value of 3.3 for the super-allowed decay branch. Jokinen et al. determined only relative branching ratios. These relative branching ratios are in nice agreement with our results except for the 1.9 MeV peak, where our branching ratio is about a factor of two too low. As explained above, this discrepancy is due to the cut-off from the trigger threshold. If we use the relative branching ratios from Jokinen et al. [17] for the 1.90 MeV and 4.61 MeV peaks and our absolute branching ratio for the 4.61 MeV peak, we obtain an absolute branching ratio of 24(5)% for the 1.90 MeV peak.

The decay-time spectrum (figure 4b) for ^{57}Zn yields a half-life of 48(3) ms. This result is in agreement with, but more precise than the result of Vieira et al. of 40(10) ms [16]. We determine a new recommended average value of 47(3) ms.

The total proton-emission branching ratio was determined by integrating the charged-particle spectrum above 2.2 MeV. The integrated number of counts we obtain is 436, equivalent to a branching ratio of 43.5(22)%. According to Jokinen et al., this corresponds to 56(12)% of all proton activity. Therefore, we determine at total proton-emission branching ratio of 78(17)%. This high value is understandable due to the fact that the β decay to the ground state of ^{57}Cu is a forbidden $7/2^- \rightarrow 3/2^-$ transition. In addition, according to the mirror nucleus of ^{57}Cu, ^{57}Ni, one expects only one particle-bound state at about 750-800 keV (there is an I^π=5/2$^-$ state at 768.5 keV in ^{57}Ni) which can be fed by an allowed transition. All other states in ^{57}Cu, which can be fed by an allowed β transition, are proton unbound.

4.2 The decay of the T_z = -3/2 nucleus ^{61}Ge

The decay-energy spectrum of ^{61}Ge is shown in figure 5a. One prominent line is observed at an energy of 3.22(6) keV. This energy may be compared to the energy given by Hotchkis et al. [18] of E_p^{cm} = 3.16(3) MeV. The error-weighted average energy for this peak is E_p^{cm} = 3.17(3) MeV. The branching ratio from our experiment for this peak is 55(6)%.

The half-life was determined to be 45(6) ms (see figure 5b). This value is in nice agreement with the half-life obtained by Hotchkis et al. [18] of 40(15) ms. The new recommended half-life value is 44(6) ms.

By integrating the charged-particle spectrum, we determine the total proton-emission branching ratio for ^{61}Ge to be 62(4)% with a number of implanted nuclei of 156(10). As there might be unobserved protons below the trigger threshold, this branching ratio is actually only a lower limit. Contrary to the case of ^{57}Zn, the transition to the ground state of ^{61}Ga is an allowed transition and can therefore collect some decay strength. In addition, other bound states can also be fed by allowed transitions and explain thus the lower proton emission branching ratio as compared to ^{57}Zn.

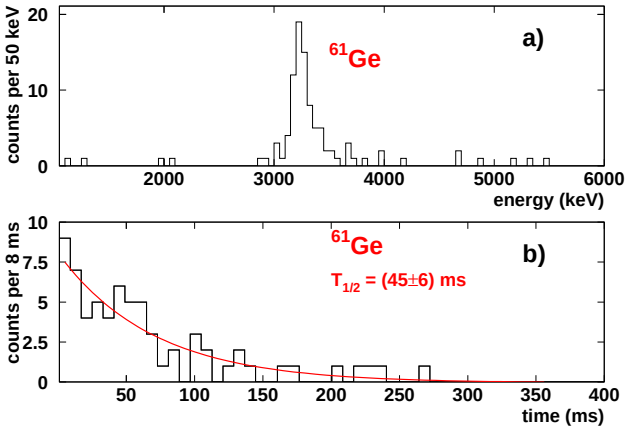

Fig. 5. a) Decay energy spectrum for ^{61}Ge. The peak is attributed to the decay of the IAS in ^{61}Ga to the ground state of ^{60}Zn. b) The decay-time distribution fitted with an exponential and a constant yields a half-life of 45(6) ms.

5 Interpretation of the decay data

To calculate the half-lives of ^{57}Zn and of ^{61}Ge, the matrix elements for the Gamow-Teller transitions were calculated using the ANTOINE code [19] and the KB3 interaction [20]. As valence space, we used the *fp* shell with an inert core of ^{40}Ca. As we have to deal with more than 12 valence particles, we used truncations of 4 for ^{57}Zn, meaning that only a maximum of 4 nucleons were allowed to be promoted from the $f_{7/2}$ orbital to the $p_{3/2}p_{1/2}f_{5/2}$ orbitals. In the case of ^{61}Ge, we used a truncation of 2. We applied a quenching factor of 0.74 for the axial-vector coupling constant. The partial half-lives for the Fermi decay were calculated using the experimental energies of the isobaric analog states.

5.1 The decay of ^{57}Zn

As in previous work [16,17], we attribute the proton line at 4.61 MeV to the decay of the isobaric analogue state of the ground state of ^{57}Zn in ^{57}Cu to the ground state of ^{56}Ni and the proton line at 1.90 MeV to the decay of the same state to the first excited state of ^{56}Ni. However, due to the low counting rate, no γ coincidences could be observed. The proton peak at 3.09 MeV belongs to the decay of a Gamow-Teller fed state at 3.79(3) MeV excitation energy in ^{57}Cu, whereas the 2.54 MeV line is due to the decay of a level at an excitation energy of 3.24(3) MeV. Both decay to the ground state of ^{56}Ni. These assignments yield a total branching ratio for the super-allowed β decay to the IAS of 43(8)%. We will use this branching ratio for the IAS below to determine the ft value.

Using a mass excess of the ^{56}Ni ground state of -53.904(11) MeV [15] and the proton energies as given above puts the IAS at a mass excess of -42.004(23) MeV and at an excitation energy of E* = 5.306(27) MeV (we used a mass excess of the ground state of ^{57}Cu of -47.310(16) MeV [15]).

This additional mass allows us to calculate the coefficients of the isobaric multiplet mass equation. We use the ground-state mass excess of ^{57}Co (Δm = -59.3442(7) MeV [15]), the

half-life (ms)	exp. result	Gross Theory [21]	Hirsch et al. [22]	ANTOINE [23]
^{57}Zn	47±3	38±4	-	29.8
^{61}Ge	44±6	39±12	45-56	9.6

Table 1. Comparison of average experimental half-lives with predictions from different models. The predictions of Hirsch et al. depend on the mass model used. The ANTOINE calculations were performed using the KB3 effective interaction [20] (see text for details).

5.239(5) MeV state in ^{57}Ni (mass excess of the ground state of -56.0820(18) MeV [15]), and the newly determined mass excess for the IAS in ^{57}Cu. The values for the IMME parameters thus obtained are a = 0.169(13) MeV, b = -8.839(24) MeV, and c = -46.466(9) MeV. These parameters allow for the determination of the ground-state mass excess of ^{57}Zn of -32.83(5) MeV. This value may be compared to the mass predictions from Audi et al. [15] of -32.8(1) MeV, to the result from the Garvey-Kelson relation [7] of -32.78(4) MeV, and to the results obtained by means of the Coulomb displacement relation [5,6], which yields -32.86(4) MeV. The Garvey-Kelson value has been recalculated using the new mass values from Audi et al. [15]. All these predictions are in nice agreement with the value obtained from the IMME, which is most likely the most reliable result.

Using the IMME, we determine a value of 9.18(5) MeV for the β-decay Q value to the IAS in ^{57}Cu. With this value, we determine the statistical rate function f to be 27400(800) s. With a partial half-life for the decay to the IAS of t = 112(22) ms, we determine an ft value for the decay of ^{57}Zn to the IAS in ^{57}Cu of 3050(600) s. Neglecting small contributions from Gamow-Teller β decay, the ft value is related to the transition strength $< BF >^2$ for a pure Fermi transition by means of the following relation:

$$ft = \frac{k}{< BF >^2}, \qquad (1)$$

where $< BF >$ is given by $\sqrt{(T+1)T - T_{Zi}T_{Zf}}$, with T being the isospin of the parent and the daughter state (T=3/2 in the present case) and T_{Zi} and T_{Zf} being the third component of the isospin for the initial as well as final nuclear state, respectively, calculated as $T_Z = (N-Z)/2$, and k=6140 s is a constant. With $< BF >^2$ =3, we determine a theoretical ft value for the decay of ^{57}Zn to the IAS in ^{57}Cu of 2047 s. To calculate this value, we neglected corrections due to isospin impurities and radiative corrections, which are usually at the few percent level. The discrepancy between the theoretical and the experimental value may either indicate that the neglected corrections are larger than assumed or that not all decay strength has been observed and the IAS decays with a small branching ratio by γ decay.

The experimental half-life of (47±3) ms may be compared (see table 1) to predictions from the Gross Theory [21] ($T_{1/2}$ = 38(4) ms) and to prediction from the ANTOINE shell-model code [23] using the KB3 effective interaction, for which we obtain a value of 29.8 ms. This large discrepancy is most likely due to the important truncation necessary to compute the half-life. A possible improvement of these calculations could also be to use an isospin-breaking interaction. However, usually the effect of an isospin-breaking interaction is by far smaller than the influence of the model space.

5.2 The decay of ^{61}Ge

The proton group observed in the present work and by Hotchkis et al. [18] has an error-weighted energy of 3.17(3) MeV. As in the work of Hotchkis et al., it is attributed to the decay of the IAS in ^{61}Ga to the ground state of ^{60}Zn. Using a ^{60}Zn ground-state mass excess of -54.188(11) MeV [15], we determine the mass excess of the IAS to be -43.74(3) MeV. The excitation energy of this state is therefore E^* = 3.35(6) MeV, where we used a ground-state mass excess of -47.09(5) MeV for ^{61}Ga. The Coulomb displacement method [5,6] allows us to estimate the mass excess of ^{61}Ge to be Δm = -34.12(5) MeV, which may be compared to a value of -33.73(30) MeV from the Audi et al. atomic mass evaluation [15]. The Garvey-Kelson relation yields a value of -34.0(2) MeV.

With a β-decay Q value determined from the values above of 9.62(6) MeV, we determine the f value to be 34125(1130) s. This value and the partial half-life for the decay to the IAS of 82(14) ms yield an ft value of 2800(500) s. This value is again slighly larger than the theoretical value of 2047 s for the super-allowed decay between the two T=3/2 analogue states.

The discrepancy between the half-life calculated with the shell model of 9.6 ms (table 1) and the experimental half-life (44(6) ms) is even larger for this nucleus than in the case of ^{57}Zn. Again, a very severe truncation necessary to achieve reasonable computing times is most likely the origin of this problem. In contrast, Gross theory and QRPA calculations yield values close to the experimental result.

6 Summary

In the present work, we have determined production cross sections for projectile fragments from ^{70}Ge fragmentation at intermediate energies. These cross sections are found to be much smaller than predicted by the EPAX formula. This result might have some influence on predictions of production cross sections for proton-rich fragments for present and future fragmentation facilities.

The decay studies performed with ^{57}Zn and ^{61}Ge allowed us to confirm the results obtained in earlier experiments at Berkeley and GSI. In addition, we could determine for the first time model-independent absolute branching ratios for the different proton groups and determine the half-life of these nuclei with improved precision. Using the IMME and Coulomb displacement energies, we could determine the mass excess of the ^{57}Zn and ^{61}Ge ground states.

We would like to thank the whole GANIL and, in particular, the LISE staff for their support during the experiment. We express our gratitude to the EXOGAM collaboration for providing us with the germanium detectors. This work was partly funded by the Conseil régional d'Aquitaine.

References

1. B. Blank *et al.*, Phys. Rev. Lett. **84**, 1116 (2000).
2. J. Giovinazzo *et al.*, Phys. Rev. Lett. **89**, 102501 (2002).
3. K. Sümmerer and B. Blank, Phys. Rev. C **61**, 034607 (2000).
4. W. Benenson and E. Kashy, Rev. Mod. Phys. **51**, 527 (1979).
5. M. S. Antony, J. Britz, and A. Pape, At. Data Nucl. Data Tab. **34**, 279 (1986).
6. M. S. Antony, A. Pape, and J. Britz, At. Data Nucl. Data Tab. **66**, 1 (1997).
7. J. Jänecke and P. Masson, At. Data Nucl. Data Tab. **39**, 265 (1988).
8. A. C. Mueller and R. Anne, Nucl. Instrum. Meth. **B56**, 559 (1991).
9. C. Dossat *et al.*, Phys. Rev. C **72**, 054315 (2005).
10. O. Tarasov, D. Bazin, M. Lewitowicz, and O. Sorlin, Nucl. Phys. **A701**, 661c (2002).
11. B. Fernandez-Dominguez *et al.*, Eur. Phys. J. **A25**, 193 (2005).
12. B. Blank *et al.*, Phys. Rev. C **50**, 2398 (1994).
13. A. Stolz *et al.*, Phys. Lett. **B627**, 32 (2005).
14. A. G. Artukh *et al.*, Z. Phys. A **303**, 41 (1981).
15. G. Audi, O. Bersillon, J. Blachot, and A. H. Wapstra, Nucl. Phys. **A729**, 3 (2003).
16. D. J. Vieira *et al.*, Phys. Lett. **B60**, 261 (1976).
17. A. Jokinen *et al.*, Eur. Phys. J. direct **A3**, 1 (2002).
18. M. A. C. Hotchkis *et al.*, Phys. Rev. C **35**, 315 (1987).
19. E. Caurier, Shell model code ANTOINE, IRES Strasbourg.
20. A. Poves and A. P. Zuker, Phys. Rep. **70**, 235 (1981).
21. T. Tachibana and M. Yamada, http://wwwndc.tokai-sc.jaea.go.jp/CN03/index.html.
22. M. Hirsch, A. Staudt, K. Muto, and H. V. Klapdor-Kleingrothaus, At. Data Nucl. Data Tables **53**, 165 (1993).
23. E. Caurier, A. P. Zuker, A. Poves, and G. Martinez-Pinedo, Phys. Rev. C **50**, 225 (1994).